A Simplified Ground Thermal Response Model for Analyzing Solar-Assisted Ground Source Heat Pump Systems

Jamie P. Fine, Hiep V. Nguyen, Jacob Friedman, Wey H. Leong, and Seth B. Dworkin*

Department of Mechanical and Industrial Engineering

Ryerson University

350 Victoria Street, Toronto, Canada

(*Corresponding author: seth.dworkin@ryerson.ca)

Abstract

Ground source heat pump systems that are installed in areas with heating or cooling dominant seasons, or in buildings with utilization characteristics that lead to a disparity in demand, often encounter challenges related to ground thermal imbalance. This imbalance can lead to long-term ground temperature changes and may cause premature system failure. This paper focuses on combining a ground source heat pump system with a solar thermal array, with the goal of eliminating the effect of ground thermal imbalance, and minimizing system lifetime cost. A thermal mass ground heat transfer model is combined with a time-stepping model to analyze the system for a variety of solar array sizes. The details associated with this modelling technique are presented, and case studies are provided to illustrate the results of the calculations for three different buildings. It is shown that increasing the solar array size can offset ground thermal imbalances, but increasing the array size also results in a larger initial system cost. An economic analysis is then carried out to determine the system lifetime cost as a function of this solar array size, and an optimal array size from an economic perspective was found. The result of the study shows that hybridizing a ground source heat pump system with a solar array produces a viable system from a technical and economic standpoint, can be used to avoid premature system failure, and can reduce system lifetime cost.

1. Introduction

1.1 Research Motivation

As global concerns with respect to climate change increase, there is growing pressure on building system designers to reduce energy consumption by improving system efficiency. There are a wide variety of efficiency improvements that can be implemented, ranging from new system hardware to sophisticated building control, but the target is typically to reduce building energy demand, and therefore energy cost. This reduction in energy demand often results in a decrease of greenhouse gas emissions from burning fossil fuels for heating a building, which is also being more heavily mandated by new emission laws in many jurisdictions. Ground source heat pump (GSHP) systems are being implemented as one of these efficiency measures since they can be designed to operate without on-site fossil fuel use, and can offer stable system efficiency year-round when compared to air source heat pumps [1].

The design of GSHP systems in heating or cooling dominant climate-zones, or for buildings with utilization characteristics that lead to a disparity in demand, often encounter challenges due to annual building load imbalances. These imbalances can cause long-term ground temperature changes from heat accumulation or depletion in the ground, which can lead to premature system failure [2]. To offset these imbalances, a geo-exchange system can be hybridized with conventional heating or cooling systems, such as natural gas boilers, such that the annual net ground heat exchange does not cause premature system failure [3] [4]. However, using fossil fuels for hybridization still results in direct CO_2 emissions from the system, and may not be sustainable for long-term use. Therefore, there is now focus on using renewable energy for GSHP hybridization,

and much of this focus is on the use of solar thermal panels since they can provide efficiencies of approximately 60% and emission-free heat at temperatures ranging from approximately 5°C to 60°C depending on weather conditions and panel selection [5]. In these systems, the interactions between the ground, heat pump, and solar array are critical to determine system performance, but these interactions are not well understood.

This paper focuses on the techno-economic analysis of a GSHP system that is hybridized with a solar thermal array, such that ground thermal-imbalance can be mitigated, and the lifetime cost of the system can be minimized. Unlike other studies in the literature, this analysis utilizes a conduction heat transfer finite element ground model to determine the effect of thermal loads on the ground. A finite element model simplification technique based on a thermal mass model is also presented, which allows for a reduction in computation times, while still delivering results within 5% of those from a detailed finite element model. Manufacturer heat pump performance data, along with a semi-empirical solar energy analysis, are used alongside this simplified model to predict overall system performance.

1.2 Existing Solar-assisted Ground Source Heat Pump Systems, and Modelling Methodologies

The use of solar energy as a replacement for conventional heat sources is increasing in popularity due to concerns over fossil fuel usage and greenhouse gas (GHG) emissions [6] [7]. Some systems use the solar thermal array as a refrigerant evaporator [8] [9], while others circulate water or a water-antifreeze mixture through the solar panel to extract sensible heat [10] [11]. Systems may also implement a thermal energy storage (TES) tank, which is used to store heated water before

circulating the water to the ground or the building [7] [12]. A statistical analysis of these studies has found that the addition of solar energy to the GSHP system can improve overall system efficiency by 10% to 20% in balanced systems, which will be used for comparison with the results of this study to ensure the reliability of the findings.

In this study, while improved system efficiency is a valuable result of using solar energy, the primary motivation for adding a solar array to the GSHP system is to replenish the thermal energy removed from the ground during winter months. The use of solar energy for this reason in an air-based thermosiphon system, coupled with a GSHP, has been shown to negate the effects of imbalanced thermal loads [13]. A flat-plate liquid solar panel system with TES was investigated for use in cold-climates, to reduce ground thermal imbalance, and the long-term efficiency of the system was shown to be stable [14]. Another study investigated the effect of adding a solar array to a three-year-old GSHP system, and it was shown that initial ground temperature decreases of 0.2°C per year can be reversed by the solar thermal energy [15]. However, these studies did not implement a detailed ground temperature model to predict long-term ground temperature changes.

Ground thermal models in the literature are typically categorized as either analytical or numerical, and are often used to predict long-term temperature changes of the ground [16]. Analytical models include the infinite line-source model, along with the cylindrical source model, and both of these models neglect vertical heat transfer [17] [18]. The resistance-capacitance approach to ground modelling is based upon an electrical circuit analogy, and can account for the interaction between the U-tube, grout, and the ground [19]. Finite element models have also been developed, and a two-dimensional model that accounts for one plane along the borehole depth has been shown to

estimate borehole heat transfer within 8% of experimental values [20]. Finite element modelling has also been carried out using three-dimensional models, which allow for prediction of variable fluid temperatures along the borehole, and can also account for fluid flow dynamics in the borehole pipe [16] [21]. However, in an on-off flowrate GSHP system, calculation of the fluid flow characteristics is not necessary and a three-dimensional numerical model that uses a heat flux term to represent the thermal load of the fluid on the ground has been validated against experimental data [22].

The work in this paper builds upon the previous solar-assisted GSHP studies by using a finite element ground model to predict the thermal response of the ground as a function of the solar-assisted GSHP system loads, and uses this response to determine system performance.

1.3 Detailed Finite Element Ground Model

In this study, a conduction heat transfer finite element model was used to determine ground temperatures in the GSHP system, as a function of the ground loads over time. This model was based upon the work completed by Law and Dworkin [22], with the modelling done using COMSOL [23]. The geometry shown in Figure 1 illustrates the dimensions and boundary conditions that were applied when using this technique.

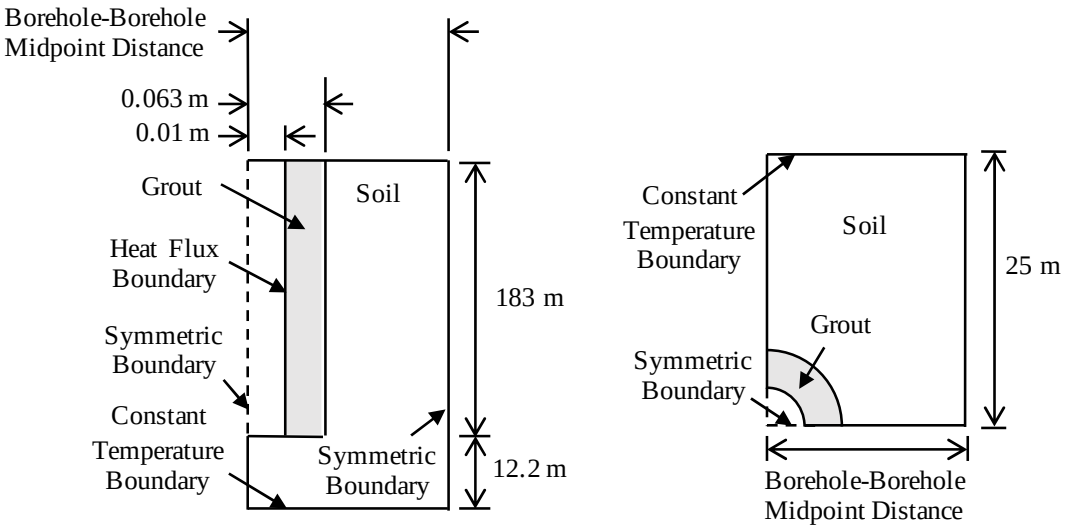

Figure 1: Schematic of COMSOL ground model geometry with boundary conditions. Cross-sectional side view (left), top view (right)

A single borehole from a multiple borehole GSHP system is included in the model, and symmetry conditions along mesh boundaries are used to replicate the effects of additional boreholes. Heat transfer in/out of the ground is included using a heat flux, which is applied along the boundary that represented the outside of the fluid-carrying pipe that is encased within a grout layer (i.e., the borehole). This heat flux is determined from building loads, which are generated using a building energy simulation, along with the performance of the heat pump in the system.

This COMSOL heat conduction model uses approximately 11,000 three-dimensional triangular prism domain elements, and 4,000 three-dimensional triangular prism boundary elements. The element starting size at the internal surface of the grout is 0.06 meters, and an element growth rate of 1.3 was used through the domain resulting in a maximum element size of 1.3 meters. The model has a wall-clock runtime of approximately 5 to 7 hours per year of simulation time on a standard

desktop personal computer. The other input parameters to the simulation are dependent on the soil and grout properties, and the parameters used in this paper will be presented in Section 3.1.

The model developed by Law and Dworkin was originally used to study the effect of different borehole layouts on ground thermal imbalance, and to determine long-term ground temperature trends for different GSHP systems. The heat source in the model was taken as a known input to the simulation process and was not calculated at each time-step based upon the interaction between the GSHP system components with the ground. This study builds upon the work by Law and Dworkin [22] by accounting for these interactions, including variable heat pump performance, variable buildings loads, and also accounts for the interactions between a solar array with the ground.

2. Analysis Technique

A time-stepping technique, combined with a thermal mass model, was used to analyze the solar-assisted GSHP system. This section will provide an overview of the system being analyzed, along with a detailed description of the analysis technique that was developed to perform the techno-economic analysis.

2.1 System Overview

A schematic of the solar-assisted GSHP system is presented in Figure 2, which includes the major system components, along with labels for important fluid states.

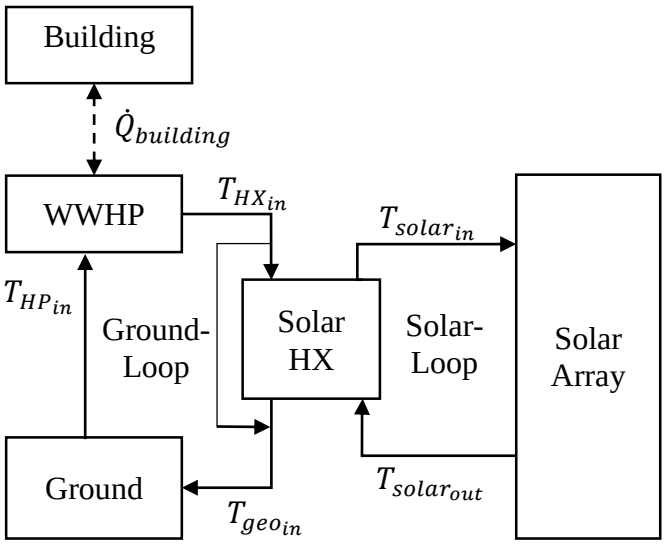

Figure 2: Solar-assisted GSHP system schematic

The building load component provides sensible heating and cooling loads as inputs to the water-to-water heat pump (WWHP). The calculation of these loads is outside the scope of this paper, and it is assumed that building loads are provided as inputs to this analysis process.

The ground component is modeled using the finite element technique, which allows for the calculation of the temperatures within the ground. This model includes a single-borehole, along with appropriate boundary conditions, to model a multi-borehole system. A detailed model is used to calibrate a simplified model, such that computational times can be reduced. The details associated with the detailed ground model are presented in Section 1.3, and the details associated with the simplification technique and simplified model are presented in Section 2.2.

The WWHP component can add/remove heat to/from the ground-fluid loop, and is used to meet building loads. Manufacturer correlations for the WWHP are used to predict the performance of this component. The details of the WWHP model are presented in Section 2.3.

The solar array component converts solar energy into heat, which is then added to the solar-fluid loop in the form of sensible energy gain. The heat generated by the solar array is a function of the operating parameters of the system, along with the solar array efficiency. The effects of pumps are not considered in this study since they are negligible compared to the solar array energy transfers and costs, as is consistent with the literature [24] [25]. The details of this model are presented in Section 2.4.

The solar heat exchanger (Solar HX) is used to transfer heat from the solar-fluid loop to the ground-fluid loop. This heat exchanger is required because potentially different fluids, and fluid flowrates, may be used in these two fluid loops. The details of the model for this component are presented in Section 2.5.

The overall system can operate in either heating or cooling mode. When the system is in heating mode, the coefficient of performance (COP) of the WWHP is determined using the heating COP correlation from manufacturer data. The WWHP will remove heat from the ground-loop fluid, which reduces the ground-loop fluid temperature. Next, the ground-loop fluid enters the solar HX, and if the outlet temperature of the solar-loop fluid from the solar array is greater than the ground-loop fluid entering the solar HX, heat will be transferred from the solar-loop fluid to the ground-loop fluid. Alternatively, the ground-loop fluid will bypass the solar HX and no heat is transferred.

The ground-loop fluid then enters the ground, and depending on the temperature difference between the ground-loop fluid and the ground there will be a resultant heat transfer, which is calculated using the technique described in Section 2.6. The ground-loop fluid leaving the ground then enters the WWHP, such that heat can be extracted at the next time-step.

Alternatively, when the system is in cooling mode, all components and control rules are the same, except that heat will be added to the ground-loop fluid by the WWHP, and the COP of the heat pump is found using the cooling COP correlation from manufacturer data. A more detailed description of this analysis technique will be presented in Section 2.7.

2.2 Simplified Ground Thermal Mass Model

Detailed simulations of the solar-assisted GSHP system, which proved to be of high computational cost, were carried out using the finite element model of the ground, as described in Section 1.3. Therefore, a computationally efficient model that could approximate the performance of the detailed model was desired.

To create this model, a simplification technique was developed, which used the detailed three-dimensional finite element COMSOL model as a calibration tool for a simplified, 4-node MATLAB thermal mass model. A difference in system performance estimation of up to 5% was deemed acceptable when comparing the detailed and simplified models. This acceptable error level was also used during model development, and resulted in the selection of a 4-node model as opposed to other node quantities. The schematic presented in Figure 3 shows the layout of the nodes and the boundary conditions that were used in the simplified model.

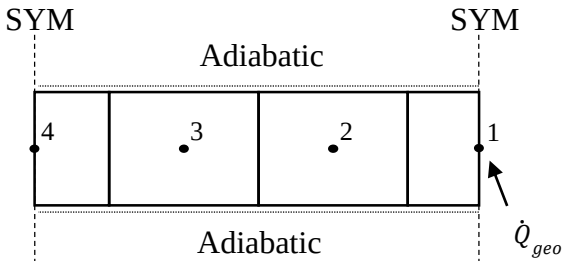

Figure 3: Simplified nodal model schematic (top view)

The heating/cooling load from the ground component in the overall system is applied to node 1, which represents the location of the borehole. Nodes 2 and 3 are used to provide thermal mass and spatial separation between nodes 1 and 4. Lastly, node 4 represents the mid-point between two boreholes in the multi-borehole system. This selection of boundary conditions allows this model to represent interior boreholes of a linear geo-field. This representation was selected since it is a conservative approach to modelling thermal imbalances in GSHP systems because a far-field and constant temperature heat sink/source is not available to dissipate/restore these imbalances [22].

Each of the nodes in the simplified model requires a thermal mass determination, and each of the node-to-node boundaries requires a product of the heat transfer coefficient and heat transfer area determination. In what follows, the product of the heat transfer coefficient and heat transfer area will be referred to as the *heat transfer coefficient product*. The thermal mass of a node relates the temperature change of that node to the internal energy change of that node over a simulation time-step. The heat transfer coefficient product between two adjacent nodes relates the temperature gradient between these nodes to the heat transfer rate between these nodes over a simulation time-step. The determination of these parameters was carried out using output data from the detailed

finite element model, which will be referred to as the *calibration* in what follows. This calibration was carried out by first determining the energy balance equation for each of the nodes in the model, as shown in Figure 4 and Equation (1).

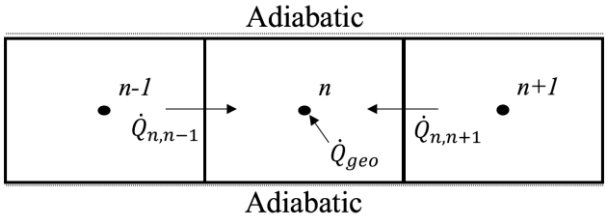

Figure 4: Node Energy Balance Schematic

$$\sum \dot{Q}_n = \dot{Q}_{n,n-1} + \dot{Q}_{n,n+1} + \dot{Q}_{geo} \quad (1)$$

where $\sum \dot{Q}_n$ is the sum of all heat transfer rates into or out of any node *n* in the simplified model, $\dot{Q}_{n,n-1}$ is the heat transfer rate into node *n* due to node *n-1*, $\dot{Q}_{n,n+1}$ is the heat transfer rate into node *n* due to node *n+1*, and $\dot{Q}_{geo}$ is the heat transfer rate into node *n* due to the borehole.

A general form of the energy balance was then derived for use with time-steps through the simulation, and is shown in Equations (2) and (3).

$$\sum_{i=j}^{k-1} \dot{Q}_i \Delta t = \sum_{i=j}^{k-1} \left[\left(\dot{Q}_{n,n+1}\right)_i + \left(\dot{Q}_{n,n-1}\right)_i + \left(\dot{Q}_{geo}\right)_i \right] \Delta t = \left(mc_p\right)_n \left(T_{n_k} - T_{n_j}\right) \quad (2)$$

$$\left(\dot{Q}_{n,x}\right)_i = (UA)_{n,x} \left(T_{x_i} - T_{n_i}\right) \quad (3)$$

where $(mc_p)_n$ is the thermal mass of node *n*, T_{n_i} is the instantaneous temperature of node *n* at time-step *i*, $(\dot{Q}_{n,x})_i$ is the heat transfer rate between node *n* and node *x* (Note: $x = n + 1$, or $x = n - 1$) at time-step *i*, $(UA)_{n,x}$ is the product of the overall heat transfer coefficient ($U_{n,x}$) and heat exchange area ($A_{n,x}$) of the ground between nodes *n* and *x*, and Δt is the length of a single time-step. In what follows, it is important to note that there may be multiple time-steps between time-steps *j* and *k*.

For node 1 as node "*n*", since it is on a symmetric boundary, the heat transfer rate from node 2 as node "*n*+1" is also the heat transfer rate from the node "*n*-1". For nodes 2, 3, and 4, the ground-loop heat injection rate is equal to zero, since that load is only applied to node 1. Lastly, for node 4, since it is also on a symmetric boundary, the heat transfer rate from node 3 is also the heat transfer rate from the node "*n*+1".

Next, using the input ground loads and output temperature results from the detailed finite element model, the thermal mass of node 1, and the heat transfer coefficient product between nodes 1 and 2 can be determined. A linear system of equations can be set up as shown in Equation (4), which is based upon Equation (2), and can be solved to yield the heat transfer coefficient product between nodes 1 and 2.

$$\begin{bmatrix} T_{1_k} - T_{1_j} & -2\Delta t \sum_{i=j}^{k-1} \left(T_{2_i} - T_{1_i}\right) \\ T_{1_z} - T_{1_k} & -2\Delta t \sum_{i=k}^{z-1} \left(T_{2_i} - T_{1_i}\right) \end{bmatrix} \begin{pmatrix} (mc_p)_1 \\ (UA)_{1,2} \end{pmatrix} = \begin{bmatrix} \Delta t \sum_{i=j}^{k-1} \dot{Q}_{geo_i} \\ \Delta t \sum_{i=k}^{z-1} \dot{Q}_{geo_i} \end{bmatrix} \quad (4)$$

where j, *k*, and *z* represent equally spaced time-steps in the detailed model simulation, such as time-step numbers j = 1, k = 3, and z = 5. In what follows, the spacing of these time-steps is defined as the *integration period*.

At this point, the thermal mass of node 2 and the heat transfer coefficient product between nodes 2 and 3 can be determined. A linear system of equations, as shown in Equation (5), can be solved to determine these parameters.

$$\begin{bmatrix} T_{2_k} - T_{2_j} & -\Delta t \sum_{i=j}^{k-1} \left(T_{3_i} - T_{2_i}\right) \\ T_{2_z} - T_{2_k} & -\Delta t \sum_{i=k}^{z-1} \left(T_{3_i} - T_{2_i}\right) \end{bmatrix} \begin{pmatrix} \left(mc_p\right)_2 \\ (UA)_{2,3} \end{pmatrix} = \begin{bmatrix} (UA)_{1,2} \Delta t \sum_{i=j}^{k-1} (T_1 - T_2)_i \\ (UA)_{1,2} \Delta t \sum_{i=k}^{z-1} (T_1 - T_2)_i \end{bmatrix} \quad (5)$$

The integration period used in this second system of equations will likely be larger than the spacing used in the first system of equations. However, tuning of the integration period can be carried out to determine values that result in acceptable simplified model predictions.

A similar process can be followed to determine the thermal mass of node 3, and the heat transfer coefficient product between nodes 2 and 3, using Equation (6).

$$\begin{bmatrix} T_{3_k} - T_{3_j} & -\Delta t \sum_{i=j}^{k-1} \left(T_{4_i} - T_{3_i}\right) \\ T_{3_z} - T_{3_k} & -\Delta t \sum_{i=k}^{z-1} \left(T_{4_i} - T_{3_i}\right) \end{bmatrix} \begin{pmatrix} \left(mc_p\right)_3 \\ (UA)_{3,4} \end{pmatrix} = \begin{bmatrix} (UA)_{2,3} \Delta t \sum_{i=j}^{k-1} (T_2 - T_3)_i \\ (UA)_{2,3} \Delta t \sum_{i=k}^{z-1} (T_2 - T_3)_i \end{bmatrix} \quad (6)$$

Similarly, the integration period used in this third system of equations will likely be larger than that used in the second system of equations.

Lastly, the thermal mass of node 4 can be determined using the relationship shown in Equation (7).

$$\left(mc_p\right)_4 = \frac{2\Delta t (UA)_{3,4}}{\left(T_{4_k} - T_{4_j}\right)} \sum_{i=j}^{k-1} (T_2 - T_3)_i \tag{7}$$

The integration period in Equation (7) will again likely be longer than that used in the third system of equations.

Once the thermal mass of each node, and the heat transfer coefficient products between each of the nodes are determined, the simplified nodal model can be used to approximate the results of the detailed model. The temperature of each node in the simplified model at each time-step, as a function of the ground heating load, can be determined using Equations (8) to (11). The initial temperatures used in the simplified model should match the inputs used to the detailed model.

$$T_{1_i} = T_{1_{i-1}} + \frac{\left[2(UA)_{1,2}\left(T_{2_{i-1}} - T_{1_{i-1}}\right) + \dot{Q}_{geo_{i-1}}\right]\Delta t}{\left(mc_p\right)_1} \tag{8}$$

$$T_{2_i} = T_{2_{i-1}} + \frac{\left[(UA)_{1,2}\left(T_{1_{i-1}} - T_{2_{i-1}}\right) + (UA)_{2,3}\left(T_{3_{i-1}} - T_{2_{i-1}}\right)\right]\Delta t}{\left(mc_p\right)_2} \tag{9}$$

$$T_{3_i} = T_{3_{i-1}} + \frac{\left[(UA)_{2,3}\left(T_{2_{i-1}} - T_{3_{i-1}}\right) + (UA)_{3,4}\left(T_{4_{i-1}} - T_{3_{i-1}}\right)\right]\Delta t}{\left(mc_p\right)_3} \tag{10}$$

$$T_{4_i} = T_{4_{i-1}} + \frac{\left[2(UA)_{3,4}\left(T_{3_{i-1}} - T_{4_{i-1}}\right)\right]\Delta t}{\left(mc_p\right)_4} \tag{11}$$

2.3 Heat Pump Performance Model

The COP of the WWHP was determined at each time-step in the simulation based upon manufacturer data. A sample heating performance table is presented in Table 1, and a sample cooling performance table is presented in Table 2.

Table 1: Sample heating COP data

	Leaving Load Hot Water Temperature (°C)					
	40			50		
Leaving Source Water Temperature (°C)	Power (kW)	Load (kW)	Heating COP	Power (kW)	Load (kW)	Heating COP
5	10	30	3	11	27.5	2.5
10	9	31.5	3.5	10	30	3
15	8	32	4	9	31.5	3.5

Table 2: Sample cooling COP data

	Leaving Load Chilled Water Temperature (°C)					
	5			10		
Leaving Source Water Temperature (°C)	Power (kW)	Load (kW)	Cooling COP	Power (kW)	Load (kW)	Cooling COP
20	8	40	5	7	42	6
25	9	36	4	8	40	5
30	10	30	3	9	36	4

The "power" value is the electrical power consumption of the compressor in the heat pump, the "load" value is the heat transfer rate to/from the heating, ventilation, and air conditioning (HVAC) system of the building when the heat pump is in heating/cooling mode respectively, and the "COP"

value represents the heating or cooling COP of the heat pump, depending on the mode of operation. Since discrete operating parameters are given in these tables, interpolation must be used, or a function can be created, that relates each of the performance parameters to the leaving water (load and source) temperatures.

The operation data in these tables can also be used to define the minimum COP operating limit of the heat pump, which is a result of a large temperature-difference between the evaporator and the condenser. For example, when the heat pump is in heating mode, the COP drops as the leaving source-water temperature drops. The *minimum* leaving source-water temperature given in these tables often coincides with the operational limit of the heat pump, which is a leaving source-water temperature of 5°C based upon the sample data in Table 1. To account for this limit, when the heat pump is in heating mode and the leaving source-water temperature is outside of this operating limit, the heat pump COP is set to 1.0. This assumption implies that an auxiliary electrical heater is used to meet the building heating load when the system is outside of the heating operating limit.

Similarly, these operating principals also apply to the heat pump when it is in cooling mode, but the limit is defined as a *maximum* leaving source-water temperature. Using the sample data presented in Table 2 to determine this limit, a maximum leaving source-water temperature of 30°C is found. However, when the system is in cooling mode and the source-water temperature is outside this limit, the heat pump is set to be inoperable, and the ground-loop fluid temperature does not change when passing through the heat pump in this case.

Alternatively, the maximum COP operating limit can be defined as when the heat pump operates with a very small temperature difference between the evaporator and condenser. As this temperature difference decreases, the COP of the heat pump increases because the pressure difference that the compressor must produce becomes small. However, to ensure that a conservative maximum heat pump performance is predicted, extrapolation beyond the maximum COP from the manufacturer table is not carried out, and the maximum COP from the performance table is used as the upper COP limit.

Using the COP from the table, along with the building loads at each given time-step, the heat being added or removed from the fluid in the ground-loop can be determined. When the system is in heating mode, the relationship shown in Equation (12) can be used to determine the heat transfer rate from the fluid in the ground-loop into the heat pump. Alternatively, when the system is in cooling mode, the relationship shown in Equation (13) can be used to determine the heat transfer rate from the heat pump into the fluid in the ground-loop.

$$\dot{Q}_{HP} = \dot{Q}_{building}\left(1 - \frac{1}{COP_H}\right) \quad (12)$$

$$\dot{Q}_{HP} = \dot{Q}_{building}\left(1 + \frac{1}{COP_C}\right) \quad (13)$$

where $\dot{Q}_{HP}$ is the heat transfer rate in/out of the ground-loop fluid, $\dot{Q}_{building}$ is the building load which is positive for cooling load and negative for heating load, COP_H is the heating COP of the heat pump, and COP_C is the cooling COP of the heat pump.

Based upon this ground-loop heat transfer rate, the temperature of the fluid in the ground-loop exiting the WWHP can be determined using Equation (14).

$$T_{HP_{out}} = T_{HX_{in}} = T_{HP_{in}} + \frac{\dot{Q}_{HP}}{\dot{m}_{geo} c_{p_{geo}}} \quad (14)$$

where $T_{HP_{out}}$ is the temperature of the fluid in the ground-loop exiting the heat pump, $T_{HX_{in}}$ is the temperature of the fluid in the ground-loop entering the solar heat exchanger, and $T_{HP_{in}}$ is the temperature of the fluid in the ground-loop entering the heat pump.

Lastly, the electrical power consumption of the heat pump can also be determined using the COP of the heat pump, as shown in Equation (15).

$$\dot{W}_{HP} = \frac{|\dot{Q}_{building}|}{COP} \quad (15)$$

where $\dot{W}_{HP}$ is the electrical power consumption of the heat pump.

2.4 Solar Panel Model

The solar panel model used in this paper is based upon the ISO standard, second-order polynomial efficiency curve, which is typically provided by manufactures for commercially available panels [26]. This efficiency curve allows the efficiency of the solar panel (η_{solar}) to be calculated based upon the inlet temperature of fluid to the panel (T_{in}), the ambient air temperature (T_a), and the total incident solar radiation (I_c). This relationship is shown in Equations (16) and (17) .

$$\eta_{solar} = \eta_0 - a_1 T_r - a_2 T_r^2 I_c \quad (16)$$

$$T_r = \frac{T_{in} - T_a}{I_c} \quad (17)$$

where η_0, a_1, and a_2 are the panel second-order efficiency parameters from the manufacturer.

The incident solar radiation on the panel is calculated using hourly solar weather data based on the geographic location of the system, and the orientation of the solar panel. The relationship shown in Equation (18) can be used to determine the total solar panel irradiation as a function of time [5].

$$I_c = I_{b,n} \cos(i_c) + I_{d,h} \cos^2\left(\frac{\beta}{2}\right) + \rho I_h \sin^2\left(\frac{\beta}{2}\right) \quad (18)$$

where $I_{b,n}$ is the beam-normal solar irradiation from the weather data, $I_{d,h}$ is the diffuse-horizontal irradiation from the weather data, ρ is the ground reflectivity, I_h is the total horizontal irradiation from the weather data, i_c is the angle between the solar irradiation vector and the panel normal, and β is the tilt angle of the panel from horizontal.

2.5 Solar Heat Exchanger Model

The solar heat exchanger is modeled using the log-mean temperature difference method, and assuming a constant heat transfer coefficient product. This technique can be applied because the ground-loop is set to operate using an on-off control scheme, and the heat transfer area of the heat exchanger will not change as the system operates. Assuming a counter-flow heat exchanger, the

heat transfer rate through the solar heat exchanger can be found using the relationship shown in Equation (19) [27].

$$\dot{Q}_{HX} = (UA)_{HX} \frac{\left(T_{solar_{out}} - T_{geo_{in}}\right) - \left(T_{solar_{in}} - T_{HX_{in}}\right)}{\ln\left(\frac{T_{solar_{out}} - T_{geo_{in}}}{T_{solar_{in}} - T_{HX_{in}}}\right)} \quad (19)$$

where $\dot{Q}_{HX}$ is the heat transfer rate of the solar heat exchanger, $(UA)_{HX}$ is the product of the overall heat transfer coefficient (U_{HX}) and heat exchange area (A_{HX}) of the solar heat exchanger, $T_{solar_{out}}$ is the temperature of the solar loop fluid exiting the solar array, $T_{solar_{in}}$ is the temperature of the solar loop fluid entering the solar array, and $T_{geo_{in}}$ is the temperature of the ground-loop fluid entering the ground.

The resulting heat transfer rate can then be used to determine the exit temperatures of both fluids from the solar heat exchanger. Equation (20) can be used for the ground-loop fluid exit temperature, and Equation (21) can be used for the for the solar-loop fluid exit temperature.

$$T_{geo_{in}} = T_{HX_{in}} + \frac{\dot{Q}_{HX}}{\dot{m}_{geo} c_{p_{geo}}} \quad (20)$$

$$T_{solar_{in}} = T_{solar_{out}} - \frac{\dot{Q}_{HX}}{\dot{m}_{solar} c_{p_{solar}}} \quad (21)$$

where $\dot{m}_{geo}$ is the mass flow rate of fluid in the ground-loop, $c_{p_{geo}}$ is the specific heat capacity of the fluid in the ground-loop, $\dot{m}_{solar}$ is the mass flow rate of fluid in the solar-loop, and $c_{p_{solar}}$ is the specific heat capacity of the fluid in the solar-loop.

2.6 Ground Heat Exchanger Model

The interaction between the ground and the ground-loop fluid is modelled using a constant surface temperature heat exchanger model, which is based upon the log mean temperature difference method [27]. The inner-wall of the borehole pipe in the ground, which is set equal to the node-1 temperature in the thermal mass model (see Section 2.2), is assumed to be isothermal, and constant over a time-step [28]. Therefore, the outlet temperature of the ground-loop fluid from the ground can be found by using the relationship shown in Equation (22).

$$T_{geo_{out}} = T_{HP_{in}} = T_{ground} - \left(T_{ground} - T_{geo_{in}}\right) \exp\left(-\frac{(UA)_{geo}}{\dot{m}_{geo} c_{p_{geo}}}\right) \quad (22)$$

where $T_{geo_{out}}$ is the exit temperature of the ground-loop fluid from the ground, $T_{geo_{in}}$ is the inlet temperature of the ground-loop fluid to the ground, T_{ground} is the effective temperature of the ground where the borehole is located, which is equal to the node 1 temperature of the simplified nodal model, and $(UA)_{geo}$ is the product of the overall heat transfer coefficient (U_{geo}) and heat exchange area (A_{geo}) of the ground heat exchanger.

2.7 Overall System Model

The overall system simulation begins by running the detailed finite element model with hourly building HVAC loads. Using the results of the detailed finite element model, and the simplification technique described in Section 2.2, the thermal masses and heat transfer coefficient products for each of the nodes and node boundaries can be determined.

Next, the parameters of the system that are constant throughout the simulation, and do not need to be re-calculated at each time-step, must be set. These parameters are shown in Table 3. A fixed solar array orientation was used since active tracking was not considered for this study.

Table 3: Constant Parameters for Overall-System Simulation

Parameter	Symbol(s)
Simulation time-step length	Δt
Weather data input file with air temperature, horizontal, diffuse-horizontal, and beam irradiation values	$T_a, I_h, I_{d,h}, \& \, I_{b,n}$
Building load file	$\dot{Q}_{building}$
Location information (longitude and latitude)	$L_{building}, l_{building}$
Solar array area	A_{solar}
Solar array tilt angle	β
Solar array azimuth angle	a_w
Solar array performance correlation	$\eta_{solar} = F(T_r, \dot{q}_{solar})$
Heat pump heating performance correlation	$COP_H = F(T_{HP_{out}})$
Heat pump cooling performance correlation	$COP_C = F(T_{HP_{out}})$
Ground-loop fluid mass flowrate when operating	$\dot{m}_{geo}$
Solar-loop fluid mass flowrate when operating	$\dot{m}_{solar}$
Specific heat capacity of fluid in ground-loop	$c_{p_{geo}}$
Specific heat capacity of fluid in solar-loop	$c_{p_{solar}}$
Heat transfer coefficient product of ground heat exchanger	$(UA)_{geo}$
Heat transfer coefficient product of the solar heat exchanger	$(UA)_{HX}$
Nodal ground heat capacities and heat transfer coefficient products	$(mc_p)_n, (UA)_{n,x}$
Ground initial temperature	$T_{ground_{init}}$

After setting the constant system parameters, all fluid temperatures in the system must be initialized to the initial ground temperature. The effect of different initial fluid temperatures was investigated using a one-year simulation, and these changes were found to have negligible effects on the annual system performance.

Next, the heat pump COP at the current time-step can be determined using the outlet temperature from the heat pump, or the outlet temperature from the previous time-step if it is not the first time-step, using the process described in Section 2.3. If the outlet temperature from the heat pump is found to be outside the heat pump operating limits, then the COP of the heat pump is set to 1.0 when in heating mode, or is considered inoperable when in cooling mode. Conversely, if the COP of the heat pump is found to be above the maximum COP operating limit, then the COP is set to the maximum rated COP of the heat pump. Using this COP, the heat transfer between the ground-loop fluid and the heat pump can be determined using Equation (12) if the system is in heating mode, or Equation (13) if the system is cooling mode.

Using this ground-loop heat transfer rate, the exit temperature of the fluid from the heat pump can be determined using Equation (14). This temperature is also equal to the temperature of the ground-loop fluid that enters the solar heat exchanger. The heat pump COP can then be used to determine the power consumption of the heat pump using Equation (15).

At this point, the performance of the solar array must be determined as a function of the current time-step fluid temperatures and weather conditions, using the process detailed in Section 2.4. This determination will yield the current time-step exit temperature of solar-loop fluid from the solar array, and the useful heat collected by the solar array. If a negative heat collection is found at the current time-step, the mass flowrate of the fluid in the solar-loop and the solar heat collection by the solar array are set to zero.

The heat transfer rate of the solar heat exchanger, along with the fluid exit temperatures from the solar heat exchanger, can be determined at this point using the process described in Section 2.5. The temperature of the fluid in the solar-loop exiting the solar array, which is equal to the temperature of the solar-loop fluid entering the solar heat exchanger, must be compared to the temperature of the fluid in the ground-loop entering the solar heat exchanger. If this solar-loop fluid temperature is greater than this ground-loop fluid temperature, and both fluid loops have a non-zero flowrate, then the solar heat exchanger will operate. Otherwise, the heat transfer rate through the solar heat exchanger is set to zero, the outlet temperatures of both fluid streams are set equal to the respective inlet temperatures of each stream, and the ground-loop fluid bypasses the solar heat exchanger.

Lastly, the heat transfer rate between the ground-loop fluid and the ground is found using the process described in Section 2.6. Based upon the resulting heat transfer rate between the ground-loop fluid and the ground, the outlet temperature of the ground-loop fluid can be determined. This heat transfer rate is then used to determine nodal temperatures using Equations (8) through (11). The flow chart presented in Figure 5 illustrates the overall simulation process.

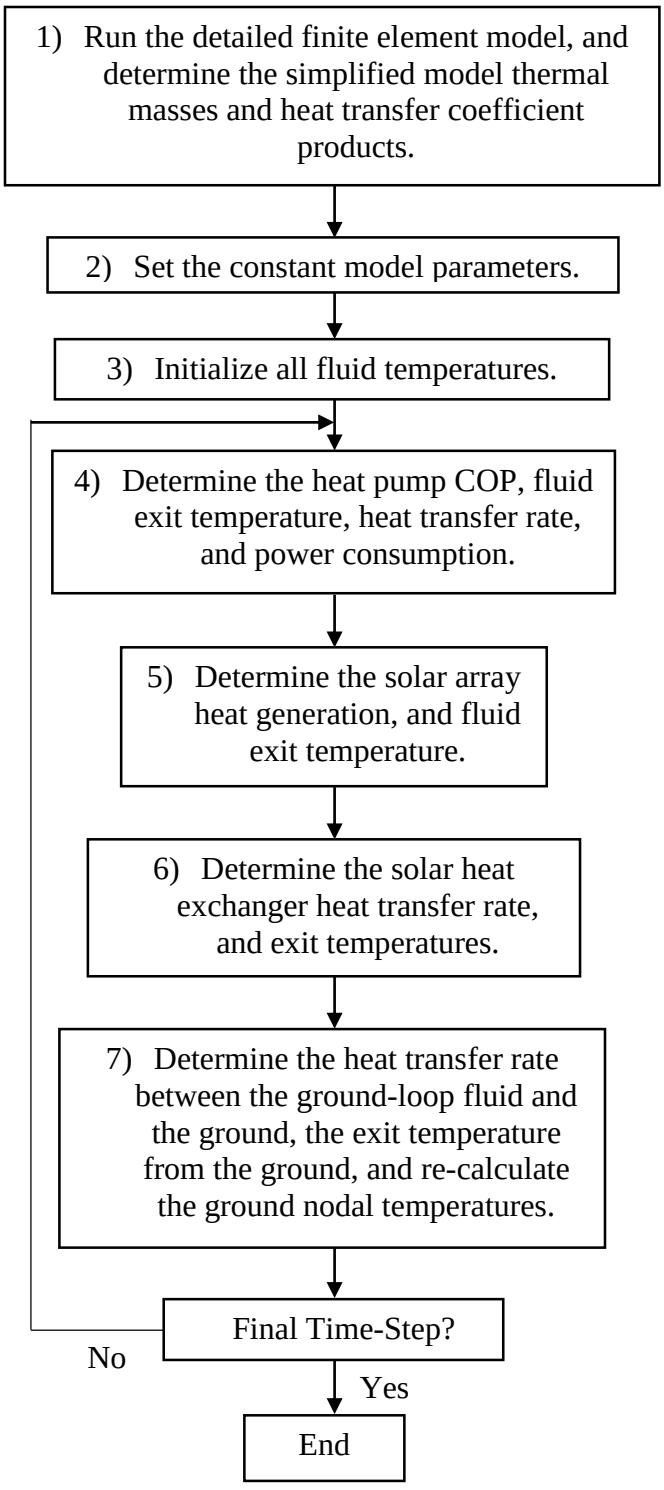

Figure 5: Overall system model flowchart

505 Steps 4 through 7, as shown in Figure 5, are repeated for each time-step in the simulation. After
506 the solution process has been carried out for the final time-step of the simulation, the analysis of
507 the system is complete. Case studies that illustrate the application of this analysis technique will
508 be presented in Section 3.
509
510
511 # 3. Model Case Study Results
512
513 This section presents case studies that were carried out using the analysis technique discussed in
514 Section 2. The details related to the energy modelling of the system are presented in Section 3.1,
515 and the economic analysis that was carried out based upon the results of the energy study are
516 presented in Section 3.2.
517
518 ## 3.1 Energy and Technical Feasibility Study
519
520 The technique described in Section 2 was used to analyze a solar-assisted GSHP system for use
521 with three different buildings in Toronto, Canada. The building loads from these buildings were
522 provided as inputs to the analysis, and were generated by a building energy simulation software
523 which is outside the scope of this study. The first building was an event space, and had an annual
524 heating-to-cooling load ratio of 20.4:1. The second building was an office, and had an annual
525 heating-to-cooling load ratio of 8.6:1. The third building was a school, and had an annual heating-
526 to-cooling load ratio of 1.2:1. These buildings were selected because of the range in building
527 heating-to-cooling ratios that they provided. Figure 6 shows the building loads for each of the

different buildings. In what follows, the start date of the simulations was taken as November 1, to represent the system being commissioned over the summer and fall, in preparation for winter.

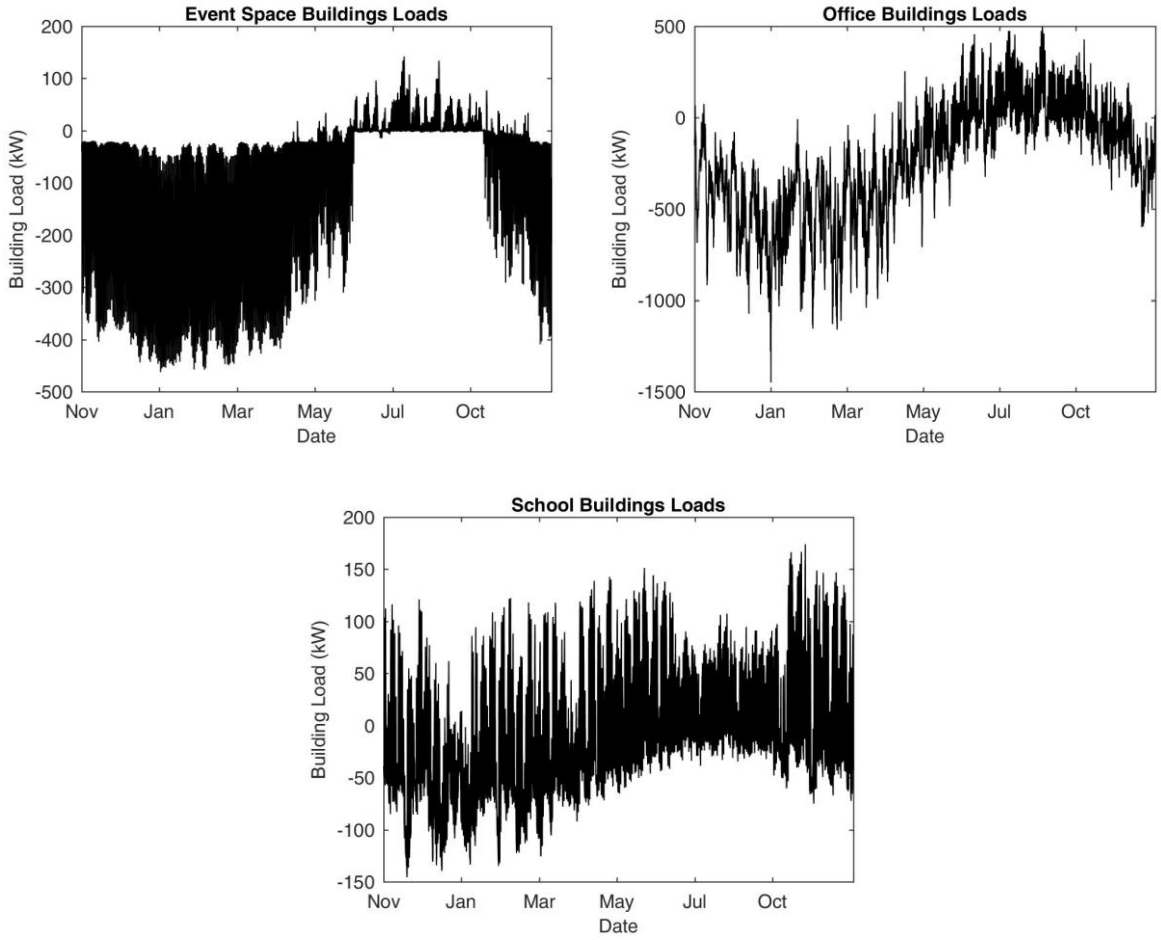

Figure 6: Case study building loads

The heat pump efficiency characteristics that were used in this study were based upon the Multistack 070NX, and the performance tables for this heat pump can be found in the product manual [29]. This heat pump model was selected based upon the building load requirements of the event venue, and normalized performance was used for each of the studies. Based upon consultation with industry, the temperature of the hot water leaving the heat pump and being sent to the building HVAC system was set to be constant at 49°C while in heating mode. Similarly,

while in cooling mode, the temperature of the chilled water leaving the heat pump and being sent to the building HVAC system was set constant at 8.9°C.

The analysis process began by first creating calibration ground-load files for use with the detailed finite element model, such that calibration temperatures for the simplified model could be generated. In these simulations, a constant heating COP of 4 was used when the system was in heating mode, a constant cooling COP of 3 when in cooling mode, and no solar panels were included. Table 4 summarizes the other input parameters to these simulations.

Table 4: Simulation input parameters for obtaining ground loads

Parameter	Value(s)	Symbols(s)
Weather data input file	Toronto CWEC Data [30]	$\rho, T_a, I_h, I_{d,h}, \& \ I_{b,n}$
Building load file	See Figure 6	$\dot{Q}_{building}$
Location information (longitude and latitude)	$43.67\ N, 79.38\ W$	$L_{building}, l_{building}$
Ground-loop fluid mass flowrate when operating	$0.25 \frac{kg/s}{ton_{peak}}$	$\frac{\dot{m}_{geo}}{\dot{Q}_{building_{peak}}}$
Specific heat capacity of fluid in ground-loop	$3449\ J/kgK$ (50/50 propylene glycol-water mix)	$c_{p_{geo}}$
Specific heat capacity of fluid in solar-loop	$3449\ J/kgK$ (50/50 propylene glycol-water mix)	$c_{p_{solar}}$
Ground initial temperature	$10°C$ [22]	$T_{ground_{init}}$
Soil conductivity	$2\ W/mK$ [22]	k_{soil}
Soil specific heat capacity	$1053\ J/kgK$ [22]	$c_{p_{soil}}$
Soil density	$1900\ kg/m^2$ [22]	ρ_{soil}
Grout conductivity	$0.7\ W/mK$ [22]	k_{grout}
Grout specific heat capacity	$1647\ J/kgK$ [22]	$c_{p_{grout}}$
Grout density	$1700\ kg/m^2$ [22]	ρ_{grout}
Solar panel area	$2.65\ m^2/panel$	A_{solar}/N_{panel}
Solar panel intercept efficiency	0.852	η_0
Solar panel efficiency slope	$3.92\ W/m^2K$	a_1
Solar panel efficiency curvature	$0.015\ W/m^2K^2$	a_2
Solar mass flow rate when operating	$0.00945\ kg/m^2s$	$\dot{m}_{solar}/A_{solar}$

These simulations were run using 1-hour time-steps, and the resulting ground loads are shown in Figure 7.

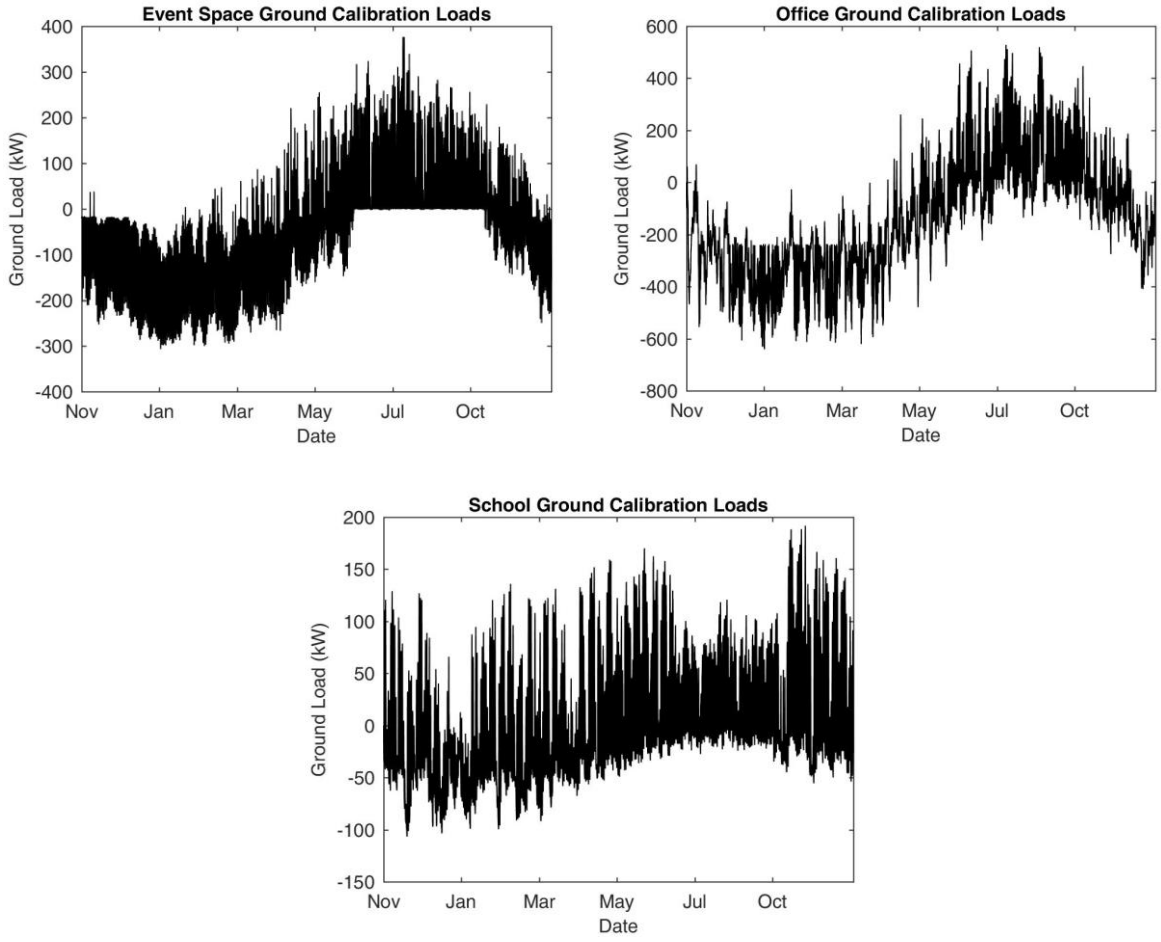

Figure 7: Calibration ground loads for nodal model

These loads were used as the input values to the detailed finite element model, and to illustrate typical results, the temperatures of the four nodes for the event space are presented in Figure 8. Node 1 contains the ground heat load and is coincident with the location of the borehole. Node 2 is one meter away from the borehole, node 3 is two meters away from the borehole, and node 4 is at the symmetric boundary conditions, which is three meters away from the borehole.

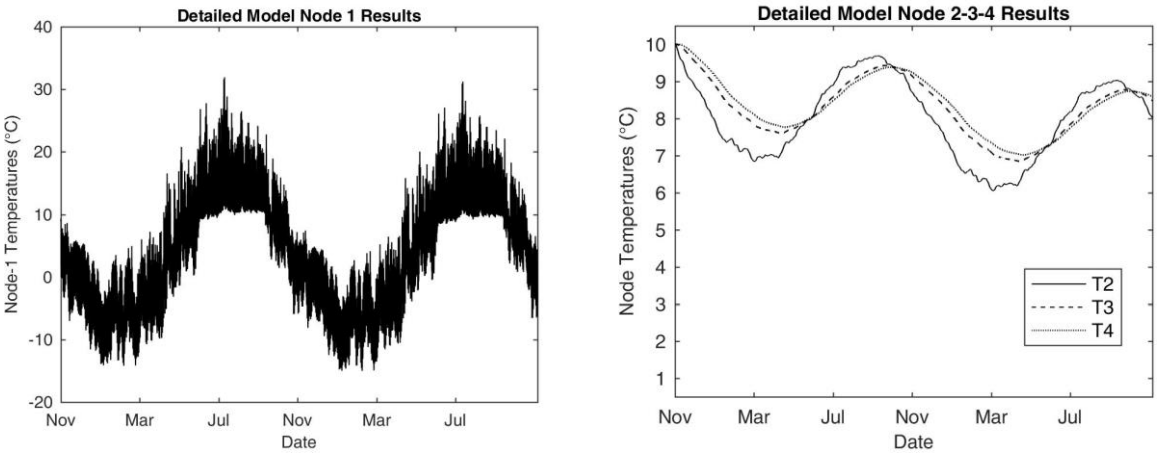

563

564 *Figure 8: Detailed finite element model node temperatures for the event-venue case*

565 The temperature arrays for all nodes from the detailed finite element model were then used to
566 calibrate the thermal mass model for each building. The integration periods for all of the nodal
567 matrix calculations, the resulting specific heat capacities based on the simplification technique as
568 shown in Equation (2), and the resulting heat transfer coefficient products as shown in Equation
569 (3) are presented in Table 5.

570

571 *Table 5: Simplified nodal heat capacities and heat transfer coefficient products*

Value	Node or Interface	Event Space	Office	School
Integration Periods (hours)	1	20	5	18
	2	150	200	150
	3	1,000	1,000	1,000
	4	17,520	17,520	17,520
Specific Heat Capacity $\left(\frac{J}{K}\right)$	1	1.38×10^8	3.82×10^8	4.56×10^7
	2	7.33×10^{10}	2.41×10^{11}	3.56×10^{10}
	3	4.60×10^{10}	4.13×10^{11}	2.55×10^{10}
	4	1.05×10^{12}	7.47×10^{12}	1.45×10^{11}
Heat Transfer Coefficient Product $\left(\frac{W}{K}\right)$	1-2	6.40×10^3	3.10×10^4	3.18×10^3
	2-3	5.29×10^4	4.36×10^5	2.39×10^4
	3-4	1.47×10^5	1.17×10^6	5.98×10^4

572

The simplified model was then run using the same calibration ground loads that were used in the detailed model, along with the nodal heat capacities and heat transfer coefficient products as shown in Table 5. Plots of the node 1 and node 4 temperatures for each of the buildings and time-steps in the calibration simulation from the detailed and simplified models are shown in Figure 9.

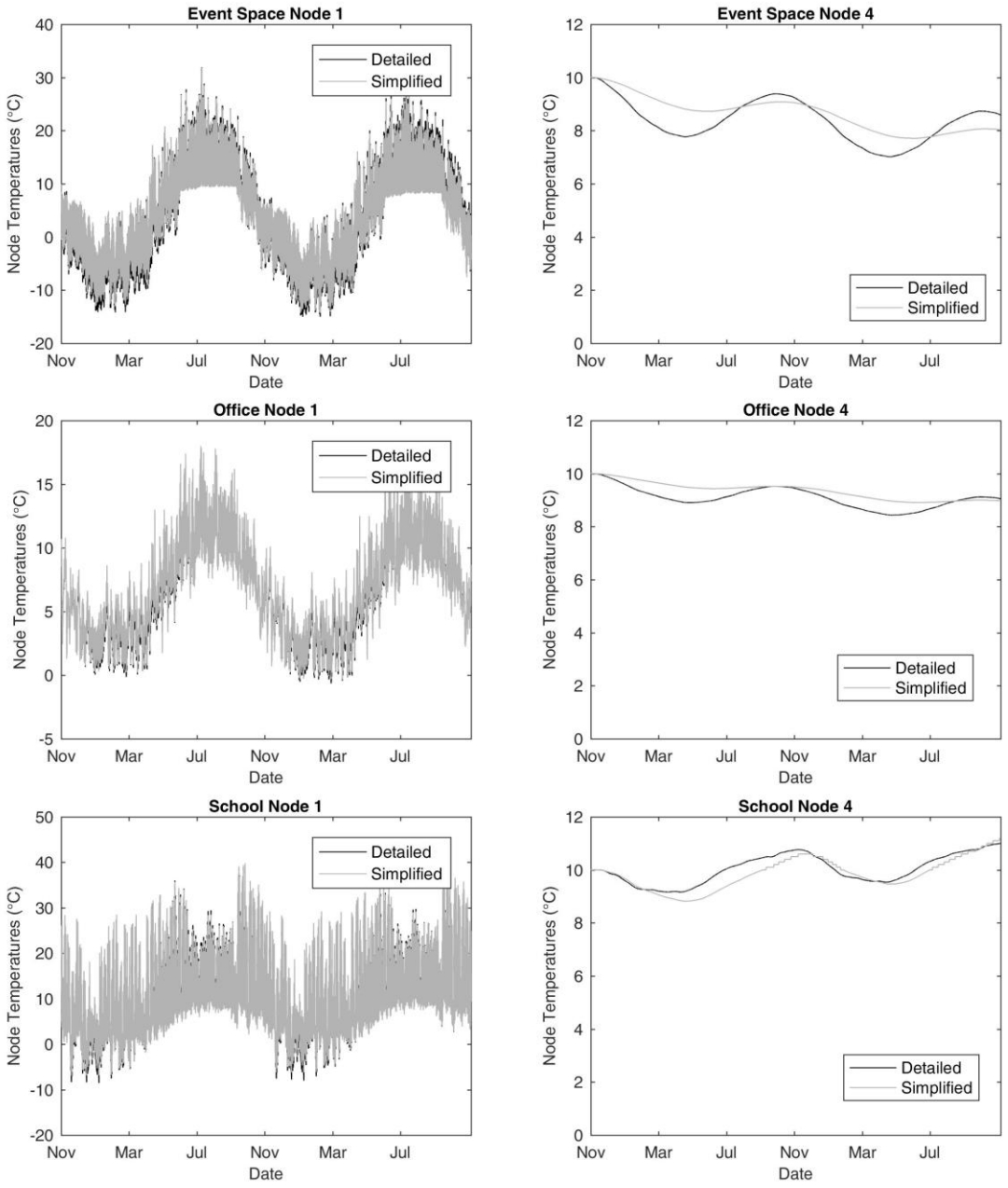

Figure 9: Comparative node 1 and node 4 temperatures from the calibration simulations

The node 1 temperature arrays from the detailed and simplified models were then used to compute the electrical energy consumption of the heat pump over the calibration period. The calculation process described in Section 2.3 was used. The resulting electrical energy consumption of the compressor for each of the models was then summed over the calibration period, and the difference between these two sums was used to check the accuracy of the calibration process. This check was carried out to validate that the simplified model can predict the same overall system performance as the detailed model, which has been definitively established, noting that the detailed model has been thoroughly validated in literature [22]. Since the end use of the simplified model is to compare the effect that different quantities of solar panels have on overall system performance, this validation is deemed to be sufficient. Other values of interest for the calibration process were the detailed model temperature range, simplified model temperature range, maximum absolute temperature difference between the two models, and the average absolute temperature difference between the two models. A summary of these results for each of the buildings is shown in Table 6.

Table 6: Summary of detailed and simplified model comparison results

Node Number	Value	Event Space	Office	School
N/A	Absolute Compressor Energy Consumption Difference	4.7%	4.8%	3.9%
1	Detailed Model Range	-14.2°C – 31.9°C	-0.15°C – 16.67°C	-8.53°C – 39.49°C
	Simplified Model Range	-13.1°C – 31.9°C	0.19°C – 17.98°C	-6.94°C – 39.83°C
	Maximum Absolute Difference	8.07°C	3.24°C	9.51°C
	Average Absolute Difference	1.96°C	0.63°C	1.61°C
4	Detailed Model Range	7.77°C –10.0°C	8.91°C – 10.00°C	9.16°C –10.0°C
	Simplified Model Range	8.49°C –10.0°C	9.43°C – 10.00°C	8.82°C –10.0°C
	Maximum Absolute Difference	0.96°C	0.8°C	0.66°C
	Average Absolute Difference	0.51°C	0.28°C	0.23°C

597 The full-system model was then run using the thermal mass parameters shown in Table 5, along
598 with the additional system parameters shown in Table 7.
599
600 *Table 7: Summary of building specific system parameters*

	Event space	Office	School
Calculated heat transfer product of ground heat exchanger (W/K)	6.86×10^4	2.15×10^5	2.58×10^4
Calculated ground-loop fluid mass flowrate when operating (kg/s)	24.9	78.0	9.36

601
602 Each run considered a new quantity of solar panels, and each simulation was run using a 40-year
603 simulation period. The ground temperatures determined using the simplified nodal model were
604 used to determine the performance of the heat pump and solar array at each time-step in the
605 simulation period, which allowed for the interaction between all system components to be
606 represented. The plots shown in Figure 10 illustrates the effect of additional solar panels on the
607 long-term temperature response of node 4 from the event space, office, and school.
608

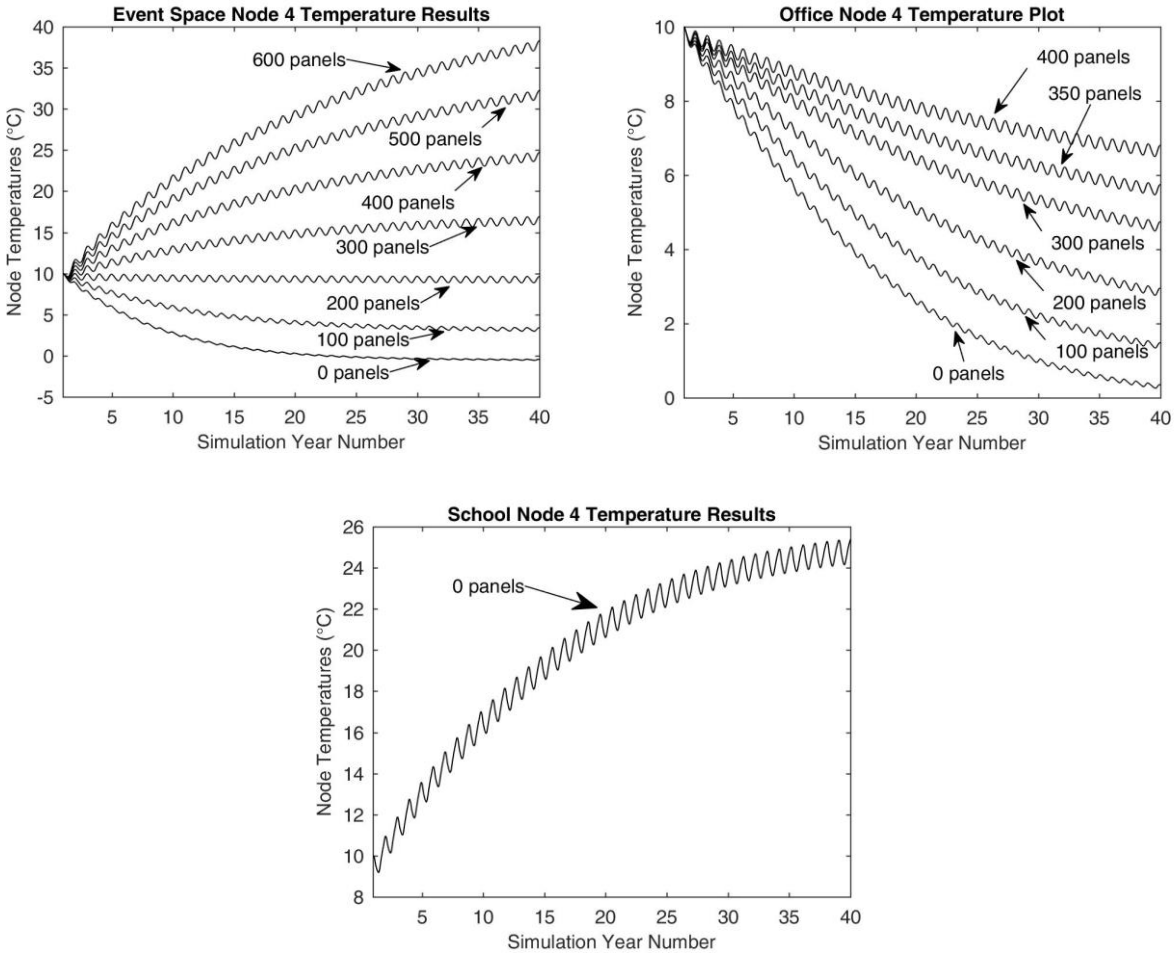

609

610

611 *Figure 10: Node 4 temperature results for different numbers of solar panels.*

612

613 The results, as shown in Figure 10, show both short-term fluctuations and long-term changes in
614 ground temperature. The short-term fluctuations are caused by the seasonal variations in ground
615 loads, which cause a decrease in ground temperature during the winter months, and an increase in
616 ground temperature during the summer months. If the annual ground loads are balanced, these
617 short-term fluctuations are approximately equal to each other, as shown by the 200-panel curve
618 for the event space in Figure 10. However, if the annual ground loads are imbalanced, then one of
619 the seasonal fluctuations will be consistently larger than the opposing seasonal fluctuation, which

will lead to a long-term temperature change. The 0-panel curve for the office in Figure 10 represents a case with winter ground temperature decreases that are consistently more than the summer temperature increases, which leads to a long-term decrease in ground temperature. This temperature decrease reduces the amount of heat that can be removed from the ground, which causes the heat pump COP to decrease, and leads to the asymptotic trend in long-term ground temperature. Conversely, as shown by the 0-panel curve for the school in Figure 10, the summer ground temperature increases are larger than the winter temperature decreases, which leads to long-term ground temperature increases.

The minimum number of panels that a system could use, while still being considered viable, is based on ground thermal imbalance as discussed in Section 1.2. In this study, the ground was considered thermally imbalanced when the operation of the heat pump was outside its minimum COP operating limit for more than 10% of the time-steps in a given simulation year. In what follows, the fraction of time-steps that the heat pump COP is below the minimum COP operating limit, for either heating or cooling, to the total number of time–steps is defined as the *imbalance factor*. Plots of the annual heating imbalance factors for each number of solar panels for the event space, office, and school are presented in Figure 11.

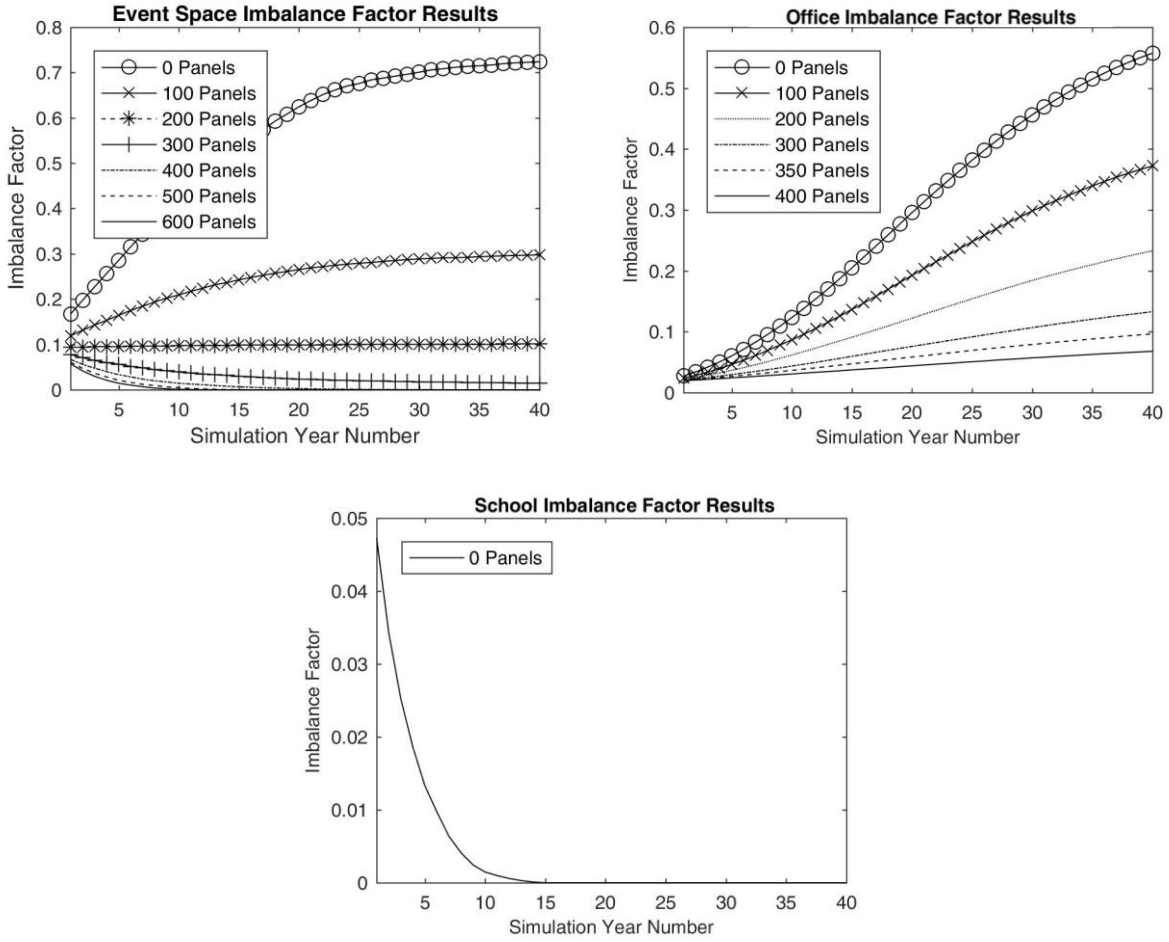

638

639

640 *Figure 11: Annual heating imbalance factors with different numbers of solar panels*

641 The results for the event space, as shown in Figure 11, show that if approximately 200 panels or
642 more are used, the system will be viable for at least 40 years based on a maximum acceptable
643 imbalance factor of 10%. However, if more than 200 panels are used, the system will experience
644 a decrease in cooling efficiency over the 40-year lifetime, since the ground will get warmer from
645 excessive heat addition, and will have a higher initial cost since more solar panels must be
646 purchased.

647 As shown in Figure 11 for the office, to ensure an imbalance factor of 10% is not exceed after 40
648 years of operation, approximately 350 solar panels are needed. It is important to note that although
649 the annual HVAC heating-to-cooling energy demand of the office is 8.6:1, compared to a ratio of

20.4:1 for the event space, that the total annual heating energy demand of the office is approximately 2.4 times larger than that of the event space. This combination of imbalanced HVAC loads and the total energy demand of the building is the overall contributor to the ground thermal response and number of solar panels that are needed.

For the school, with an annual heating-to-cooling load ratio of 1.2:1, no solar panels are needed to ensure the school does not exceed an imbalance factor of 10%. This result occurs since the HVAC energy demands of the school result in net positive heat transfer to the ground, and the long-term temperature change of the ground does not negatively impact the system COP over a 40-year lifetime. Therefore, a solar-assisted GSHP system does not need to be recommended for buildings with a 1.2:1 heating-to-cooling load ratio.

A comparison between the results of this study to the results of a similar study by Emmi *et al.* [14] has also been carried out to determine the reliability of this model when estimating overall system performance. The study by Emmi *et al.* investigated using a solar-assisted GSHP system to reduce the total borehole length required for a system. Their results presented a relationship between the solar array size and the minimum temperature of the fluid entering the ground heat exchanger each year in the simulation. The results of this comparison showed that there are matching trends in fluid temperatures entering the borehole field when adding solar panels, and that there is an ability to alleviate ground thermal imbalance by adding solar panels. However, in contrast to the present study, the study by Emmi *et al.* only investigated a single solar array size for each building, and did not investigate the impact of different array sizes for individual buildings.

Using these results, a financial study was carried out for the event space and office, since only these two buildings require solar panels to avoid ground thermal imbalance. The economic impact of purchasing panels beyond the minimum number required to avoid ground thermal imbalance was investigated, and the details of this analysis will be discussed in Section 3.2.

3.2 Economic Analysis

The economic analysis of the solar-assisted GSHP system was carried out using a net-present cost (NPC) analysis method. The NPC method converts all costs to present day values, which allows for an equal comparison between systems that have variable operating costs over the lifetimes of the systems. The system parameters that result in the lowest net-present cost is typically the most preferable if the system is fit for purpose over its lifetime, and if the upfront cost of that system is within the budget of the specific project. The relationship shown in Equation (23) can be used to determine the NPC of an installation [31].

$$NPC = C_0 + \sum_{t=1}^{n} \frac{C_t}{(1+i)^t} \tag{23}$$

where NPC is the net-present cost of the system in present day dollars, C_0 is the upfront cost of the system in present day dollars, n is the number of years being considered for the economic study, C_t is the annual operating cost of the system in year t in year t dollars, and i is the overall discount rate used for the analysis.

The upfront cost of the system (C_0) was taken as the sum of the solar panel and the solar panel installation cost. The GSHP and additional HVAC system component costs were not included in the economic analysis because these costs are not directly related to the solar array size, and therefore are not required for comparative purposes. The solar panel unit cost varied depending on the quantity that was ordered, as shown in Figure 12. The installation cost per panel was taken as a constant value at 1.2 times the cost of the solar panels. Both of these costing parameters were based upon a costing estimate from industry, quoted recently in Ontario, Canada.

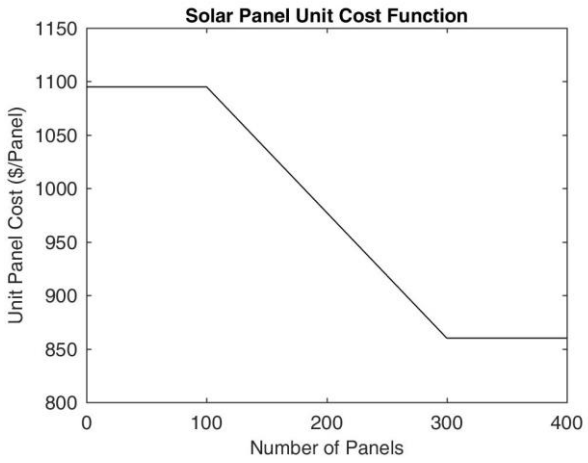

Figure 12: Solar panel costing function

The electrical cost used for this study was assumed to be $0.12 per kWh. In Ontario, Canada, the average inflation rate from 2012-2016 was 3.36% [32], but the electric utility rate has a historical growth rate of 4.26% per year [33]. Therefore, since all of the future costs being considered in this economic study are based upon electric utility costs, these two rates must be combined to determine the overall discount rate for the future costs, as shown in Equation (24).

$$i = \frac{1 + electric\ utility\ growth\ rate}{1 + economic\ inflation\ rate} - 1 = \frac{1 + 0.0426}{1 + 0.0336} - 1 = 0.87\% \qquad (24)$$

An economic assessment using a 20-year system lifetime and 40-year system lifetime was carried out for both the event space and office. The capital costs of solar panels with installation, total heat pump electrical costs, installation NPCs, average installation returns on investment (ROI), and the solar array payback periods are presented in Table 8 for the event space, and

Table 9 for the office. The electricity consumption of the heat pump was found using Equation (15) as a function of the varying ground temperature, building load, and solar energy collection, which allowed for the economic impact of the combined system to be represented. A plot of the NPC results is also shown in Figure 13.

Table 8: Event space economic study results summary

		20-Year Lifetime			40-Year Lifetime			
Number of Solar Panels	Total Capital Cost ($)	Electrical Cost (Today's $)	Total Net-Present Cost ($)	Average Annual ROI	Electrical Cost (Today's $)	Total Net-Present Cost ($)	Average Annual ROI	Payback Period (years)
0	-	2,035,000	2,035,000	N/A	4,950,000	4,950,000	N/A	N/A
100	241,000	1,524,000	1,765,000	11%	3,606,000	3,847,000	14%	13
200	430,000	1,155,000	1,585,000	10%	2,540,000	2,970,000	14%	13
300	568,000	926,000	1,494,000	10%	1,891,000	2,459,000	13%	13
400	757,000	806,000	1,563,000	8%	1,613,000	2,370,000	11%	15
500	946,000	747,000	1,598,000	7%	1,512,000	2,363,000	9%	17
600	1,135,000	719,000	1,854,000	6%	1,472,000	2,607,000	8%	19

Table 9: Office economic study results summary

		20-Year Lifetime			40-Year Lifetime			
Number of Solar Panels	Total Capital Cost ($)	Electrical Cost (Today's $)	Total Net-Present Cost ($)	Average Annual ROI	Electrical Cost (Today's $)	Total Net-Present Cost ($)	Average Annual ROI	Payback Period (years)
0	-	3,189,000	3,189,000	N/A	8,938,000	8,938,000	N/A	N/A
100	241,000	2,879,000	3,119,000	6%	7,773,000	8,014,000	12%	18
200	430,000	2,629,000	3,059,000	7%	6,767,000	7,197,000	13%	18
300	568,000	2,429,000	2,997,000	7%	5,935,000	6,503,000	13%	18
400	757,000	2,267,000	3,024,000	6%	5,269,000	6,026,000	12%	19
500	946,000	2,141,000	3,087,000	6%	4,756,000	5,702,000	11%	20
600	1,135,000	2,044,000	3,179,000	5%	4,395,000	5,530,000	10%	20
700	1,324,000	1,969,000	3,293,000	5%	4,150,000	5,475,000	9%	21
800	1,514,000	1,912,000	3,426,000	4%	3,992,000	5,506,000	8%	22

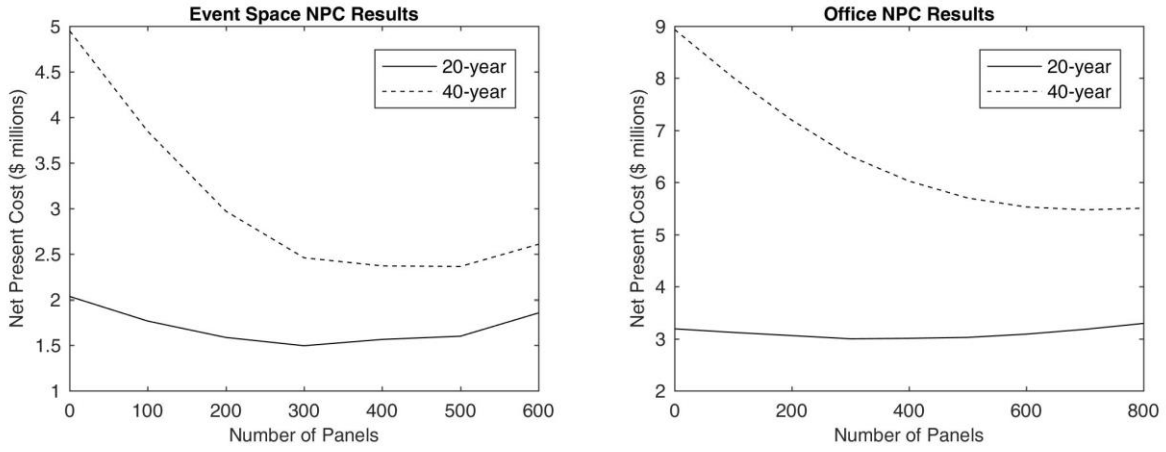

Figure 13: Plot of NPC for the event space and office

The economic study results show that as the number of solar panels initially increases, the NPC of the system decreases for both buildings. This decrease occurs because as more solar panels are added, the ground temperature tends to increase over time, which boosts the annual average heating COP of the system. This boost results in a decreased energy consumption, and energy cost, during the heating months. However, as the ground temperature increases, the increasing heating COP effects begin to diminish, and the annual average cooling COP decreases. The solar panels also operate at higher efficiency when lower quantities are used, since the overall system temperatures

738 are lower than if more panels are used, which also results in additional solar panels exhibiting
739 diminishing benefit for the system.
740
741 The results of the economic study also show that longer system lifetimes tend to favour a larger
742 number of solar panels compared to shorter system lifetimes, for both buildings. This result occurs
743 because the energy, and therefore cost, savings that are realized due to the addition of more solar
744 panels continues throughout the lifetime of the system. Longer system lifetimes then allow for
745 larger savings from the same initial investment, which results in large solar arrays becoming
746 economical with longer system lifetimes.
747
748 Lastly, the optimal number of solar panels may be different than the number of panels that results
749 in no long-term ground temperature changes. For example, the event space requires approximately
750 200 panels to avoid long-term ground temperature changes, but approximately 500 panels are
751 optimal based on a 40-year NPC analysis. This difference can be attributed to the initial ground
752 temperature in the case study of 10˚C, and a selection of 500 panels resulting in the far-field ground
753 temperature to by 22˚C over 40 years. In this case, while the temperature rise may be impractically
754 high, this combination of initial ground temperature and temperature rise results in heating
755 performance improvements that offset the reductions in cooling performance, which offsets the
756 cost associated with purchasing additional solar collectors. Therefore, one must consider technical
757 factors such as building load profile, initial ground temperature, and heat pump operation, along
758 with solar panel mounting area, and upfront cost constraints when determining the optimal number
759 of solar panels using the NPC analysis.
760

4. Conclusion

In this study, a model that couples a solar-assisted GSHP system with a simplified ground heat transfer model to determine long-term system performance was presented. The motivation for the study was to develop an approach to determine the number of solar panels required to avoid premature system failure due to ground thermal imbalance, along with determining the economic impact of varying the number of solar panels for a given building and GSHP system. Unlike previous studies in the literature, this study included a thermal mass model to predict ground temperatures over time, as a function of building and solar loads.

Initially, a detailed finite element numerical model in COMSOL was used to determine the thermal response of the ground, but because computation times were approximately 5 to 7 hours of wall-clock time per year simulated, a simplified 4-node thermal mass model was created. This simplified model used calibration data from the detailed model and produced annual energy consumption differences of less than 5% when compared to the detailed model. Three buildings were investigated for use with the solar-assisted GSHP system, which had heating-to-cooling load ratios of 20.4:1, 8.6:1, and 1.2:1. Simulation results showed that the school, with a load ratio of 1.2:1, was not suitable for hybridization because the imbalance factor with no solar panels was less than 10%. However, the results of the energy simulations from the event space and office showed that solar panels were needed to avoid exceeding the maximum imbalance factor of 10%. The event space, which had a heating-to-cooling load ratio of 20.4:1, required approximately 200 panels to avoid exceeding the 10% imbalance factor limit. The office building, which had a heating-to-cooling load ratio of 8.6:1, required approximately 350 panels based upon the same imbalance factor limit. Based upon these results, it was found that the quantity of panels required

for both buildings was a function of both the total building energy consumption, and the building load ratios.

An economic analysis was then carried out for both the event space and office building, and the results showed that an optimal number of panels could be found using the presented NPC analysis technique. For the event space, the optimal quantities were 300 panels for a 20-year system lifetime, and 500 panels for a 40-year system lifetime, which differed from the quantity required based upon the imbalance factor limit. Similarly, the optimal quantities for the office building were found to be 300 and 700 panels for 20-year and 40-year system lifetimes, respectively, which also differed from the quantity determined using the imbalance factor limit. It was determined that these trends were exhibited because as the quantity of solar panels initially increased, the heat pump heating efficiency augmentations from the solar array resulted in decreased total energy consumption, which offset the cost of additional solar panels. However, as the quantity of solar panels continued to increase, and because the efficiency of a solar panel diminishes with increasing operating temperature, solar panel efficiency decreased. Similarly, there is also a reduction in heat pump cooling performance as more solar collectors are added, which also begins to offset the heating performance increases. Therefore, these three factors combine to generate an economically optimal point for a given system.

Furthermore, this study has shown that solar-assisted GSHP systems need careful attention to ensure that they remain viable from economic and technical viewpoints. Using a simplified ground model with a solar-assisted GSHP system model is a suitable method to determine this viability.

Acknowledgements

This research was undertaken, in part, thanks to funding from the Canada Research Chairs program. We would also like to acknowledge the Natural Sciences and Engineering Research Council of Canada, and the Ontario Graduate Scholarship program for funding towards this research.

Works Cited

[1] M. Mohanraj, Y. Belyayev, S. Jayaraj and A. Kaltayev, "Research and developments on solar assisted compression heat pump systems – A comprehensive review (Part-B: Applications)," vol. 83, pp. 124-155, 2018.

[2] S. Hu, W. Song, Y. Zhang, D. Pan and T. Meng, "Study of Cold/Hot Stacking Problem Based on Balance Storage of Ground Source Heat Pump," in *2nd International Conference on Computer Engineering and Technology*, 2017.

[3] Y. Man, H. Yang and J. Wang, "Study on hybrid ground-coupled heat pump system for air-conditioning in hot-weather areas like Hong Kong," *Applied Energy,* vol. 9, no. 87, pp. 2826-2833, 2010.

[4] J. Meyer, D. Pride, J. O'Toole, C. Craven and V. Spencer, "Ground-Source Heat Pumps in Cold Climates," 31 May 2011. [Online]. Available: http:// www.cchrc.org/sites/default/files/docs/Ground-Source-Heat-Pumps-in-Cold-Climates.pdf. [Accessed 24 July 2017].

[5] J. P. Fine, J. Friedman and S. B. Dworkin, "Detailed modeling of a novel photovoltaic thermal cascade heat pump domestic water heating system," *Renewable Energy,* no. 101, pp. 500-513, 2017.

[6] V. Devabhaktuni, M. Alam, S. Shekara Sreenadh Reddy Depuru, R. C. I. Green, D. Nims and C. Near, "Solar energy: Trends and enabling technologies," *Renewable and Sustainable Energy Reviews,* no. 19, pp. 555-564, 2013.

[7] M. Mohanraj, Y. Belyayev, S. Jayaraj and A. Kaltayev, "Research and developments on solar assisted compression heat pump systems – A comprehensive review (Part A: Modeling and modifications)," *Renewable and Sustainable Energy Reviews,* vol. 83, pp. 90-123, 2018.

[8] M. Hawlader, S. Chou and M. Ullah, "The performance of a solar assisted heat pump water heating system.," *Applied Thermal Engineering,* no. 21, pp. 1049-1065, 2001.

[9] A. Moreno-Rodriguez, N. Garcia-Hernando, A. Gonzalez-Gil and M. Izquierdo, "Experimental validation of a theoretical model for a direct-expansion solar-assisted heat pump applied to heating," *Energy,* vol. 60, pp. 242-253, 2013.

[10] Y. Bi, T. Guo, L. Zhang and L. Chen, "Solar and ground source heat-pump system," *Applied Energy,* no. 78, pp. 231-245, 2004.

[11] D. Lanhua, L. Sufen, D. Lin, L. Xiangli, S. Yan and D. Ming, "Experimental performance analysis of a solar assisted ground source heat pump system under different heating operation modes," *Applied Thermal Engineering,* vol. 75, pp. 325-333, 2015.

[12] Y. Kuang, R. Wang and L. Yu, "Experimental study on solar assisted heat pump system for heat supply.," *Energy Conversion and Management,* no. 44, pp. 1089-1098, 2003.

[13] T. You, B. Wang, W. Wu, W. Shi and X. Li, "Performance analysis of hybrid ground-coupled heat pump system with multi-functions," *Energy Conversion and Management,* no. 92, pp. 47-59, 2015.

[14] G. Emmi, A. Zarrella, M. De Carli and A. Galgaro, "An analysis of solar assisted ground source heat pumps in cold climates," *Energy Conversion and Management,* no. 106, pp. 660-675, 2015.

[15] N. Zhu, J. Wang and L. Liu, "Performance evaluation before and after solar seasonal storage coupled with ground source heat pump," *Energy Conversion and Management,* vol. 103, pp. 924-933, 2015.

[16] H. Biglarian, M. Abbaspour and M. H. Saidi, "Evaluation of a transient borehole heat exchanger model in dynamic simulation of a ground source heat pump system," *Energy,* vol. 147, pp. 81-93, 2018.

[17] H. Biglarian, M. Abbaspour and M. H. Saidi, "A numerical model for transient simulation of borehole heat exchangers," *Renewable Energy,* vol. 104, pp. 224-237, 2017.

[18] A. Zarrella, G. Emmi and M. De Carli, "A simulation-based analysis of variable flow pumping in ground source heat pump systems with different types of borehole heat exchangers: A case study," *Energy Conversion and Management,* vol. 131, pp. 135-150, 2017.

[19] M. De Carli, M. Tonon, A. Zarrella and R. Zecchin, "A computational capacity resistance model (CaRM) for vertical ground-coupled heat exchangers," *Renewable Energy,* vol. 35, pp. 1537-1550, 2010.

[20] S. J. Rees, "An extended two-dimensional borehole heat exchanger model for simulation of short and medium timescale thermal response," *Renewable Energy,* vol. 83, pp. 518-526, 2015.

[21] L. Pu, D. Qi, K. Li, H. Tan and Y. Li, "Simulation study on the thermal performance of vertical U-tube heat exchangers for ground source heat pump system," *Applied Thermal Engineering,* vol. 79, pp. 202-213, 2015.

[22] Y. L. E. Law and S. B. Dworkin, "Characterization of the effects of borehole configuration and interference with long term ground temperature modelling of ground source heat pumps," *Applied Energy,* no. 179, pp. 1032-1047, 2016.

[23] COMSOL Inc., "COMSOL Multiphysics," 2017. [Online]. Available: www.comsol.com.

[24] O. Ozgener and L. Ozgener, "Modeling of driveway as a solar collector for improving efficiency of solar assisted geothermal heat pump system: a case study," *Renewable and Sustainable Energy Reviews,* no. 46, pp. 210-217, 2015.

[25] M. A. Lambert and A. Beyene, "Thermo-economic analysis of solar powered adsorption heat pump," *Applied Thermal Engineering,* no. 27, pp. 1593-1611, 2007.

[26] J. P. Fine, J. Friedman and S. B. Dworkin, "Transient analysis of a photovoltaic thermal heat input process with thermal storage," *Appied Energy,* vol. 160, pp. 308-320, 2015.

[27] Y. A. Çengel and A. J. Ghajar, Heat and mass transfer: fundamentals and applications, New York: McGraw-Hill, 2011.

[28] S. Lazzari, A. Priarone and E. Zanchini, "Long-term performance of BHE (borehole heat exchanger) fields with negligible groundwater movement," *Energy,* vol. 35, pp. 4966-4974, 2010.

[29] Multistack, "Multistack Water to Water Heat Pump Catalog for R410 or R134a Refrigerant," 2017. [Online]. Available: https://www.google.ca/url?sa=t&rct=j&q=&esrc=s&source=web&cd=2&cad=rja&uact=8&ved=0ahUKEwjnx7HDpbbVAhUC04MKHZKJD58QFgg6MAE&url=http%3A%2F%2Fwww.multistack.com%2FPortals%2F0%2FLiterature%2FCatalogs%2FWater%2520To%2520Water%2520Heat%2520Pump%2520Catalog.pdf&usg=AFQjCNG5NPVgFz-hr6aShgoqsOe-5VSHQg. [Accessed 21 May 2017].

[30] Meteorological Service of Canada and The National Research Council of Canada, "Canadian Weather Energy and Engineering Data Sets (CWEEDS Files)," The National Research Council of Canada, Ottawa, 2008.

[31] D. G. Newnan, J. P. Lavelle and T. G. Eschenbach, Engineering Economic Analysis (10th Edition)., Oxford University Press, 2009.

[32] Statistics Canada, "Consumer Price Index, by province (Ontario)," Government of Canada, 20 January 2017. [Online]. Available: http://www.statcan.gc.ca/tables-tableaux/sum-som/l01/cst01/econ09g-eng.htm. [Accessed 2 August 2017].

[33] D. D. Dewees, "Background Report: What Is Happening to Ontario Electricity Prices?," University of Ottawa, Ottawa.

[34] ISO, "Solar energy-Solar thermal collectors-Test methods ISO/FDIS 9806:2013(E)," Geneva, 2013.

[35] Aermec, "Aermec NRL Chiller Datasheet," Aermec S.p.A, Rome, Italy.

[36] E. Bellos, C. Tzivanidis, K. Moschos and K. A. Antonopoulos, "Energetic and financial evaluation of solar assisted heat pump space heating systems," *Energy Conversion and Management,* vol. 120, pp. 306-319, 2016.

[37] S. Gehlin, "Thermal response test - Method development and evaluation - PhD Thesis," Luleå University of Technology, 2002.

[38] H. Carslaw and J. Jaeger, Conduction of Heat in Solids, Oxford University Press: Oxford, 1959.

[39] S. Javed and P. Fahlen, "Thermal Response Testing of a Multiple Borehole Ground Heat Exchanger," in *SET2010 - 9 th International Conference on Sustainable Energy Technologies*, Shanghai, 2010.

[40] R. A. Beier, M. D. Smith and J. D. Spitler, "Reference data sets for vertical borehole ground heat exchanger models and thermal response test analysis," *Geothermics,* vol. 40, pp. 79-85, 2011.

816

817